PHYSICAL REVIEW E **68**, 021805 (2003)

Effects of geometric confinement on the adhesive debonding of soft elastic solids

Rebecca E. Webber and Kenneth R. Shull
Department of Materials Science and Engineering, Northwestern University, Evanston, Illinois 60208, USA

Alexandra Roos and Costantino Creton
Laboratoire de Physicochimie et Macromoleculaire, Ecole Superieure de Physique et de Chimie Industrielles, Paris, France

(Received 23 January 2003; published 29 August 2003)

The effect of increasing confinement on soft elastic gel layers has been investigated and a means of analyzing the behavior of such systems has been developed. A probe tack test was used to study the behavior of thin elastic layers during interfacial debonding from a cylindrical glass indenter. For this gel-indenter system, confinement is defined as the ratio of a_0, the radius of the indenter, to h, the thickness of the elastic layer. In order to investigate geometric effects, the adhesion energy of the gel was kept constant while the thickness and modulus of the gels were varied. A fracture mechanics approach, based on the compliance of the layer, has been employed in analyzing the experimental data. It is shown that a fracture mechanics analysis is appropriate for these systems, allowing quantitative results to be obtained, despite very irregular contacts. It has also been shown that the interfacial instabilities observed during debonding maximize the compliance of the elastic layer. Additionally, four dimensionless parameters that dictate the behavior of confined systems have been defined, offering a general guide to understanding and characterizing the mechanical behavior of thin elastic layers.

DOI: 10.1103/PhysRevE.68.021805 PACS number(s): 82.35.Gh, 81.70.Bt, 46.32.+x, 68.35.Gy

I. INTRODUCTION

Understanding the behavior of thin, compliant layers is of vital importance in a wide variety of applications, including pressure sensitive adhesives [1] and hydrogel bioadhesives [2]. The deformation behavior of thin, compliant materials is dependent not only on material properties, but also on the confinement of the layer, which can be expressed as a ratio of the lateral dimensions of the adhesive layer to its thickness [3–7]. The relationship between confinement and deformation has been investigated in Newtonian fluids [8–10], viscoelastic fluids [11], and yield stress fluids [12–14], with the Saffman-Taylor instability [15] being the classic example of work in this area. The adhesive debonding behavior of confined elastic systems has also been explored and fingerlike bulk instabilities, similar to those seen in fluids, have been observed in elastic gels strained in tension [5,7,16]. The emphasis in these systems has been on the characterization and prediction of bulk elastic instabilities during debonding. However, an area of current interest involves the interfacial debonding behavior of compliant elastic systems [3,4,6]. Ghatak *et al.* [3] and Mönch and Herminghaus [6] have investigated the fingerlike instabilities that appear at the interface between a rigid substrate and a thin, elastic film using nonaxisymmetric geometries. The wavelengths of these instabilities are linearly related to the thickness of the elastic layer [3,4,6]. A better understanding of the underlying physics of this phenomenon can be achieved with additional test methods. Here, a method of analysis based on stress distribution and material compliance considerations is introduced to describe the interfacial debonding phenomena observed in soft, confined elastic layers. We focus specifically on the transition from circular edge crack propagation to interfacial crack fingering as the system confinement increases. Such a situation is representative of the practical case where a soft elastic or viscoelastic layer is confined between weakly adhering surfaces.

It has been shown that the bulk fingering instabilities in thin elastic layers are not the result of plastic yielding or viscous flow; they originate instead from the elastic nature of the material [3–6]. The geometry of a flat punch contacting a thin gel layer, shown in Fig. 1, is useful for fundamental studies of these instabilities. This geometry provides a well-defined initial contact radius corresponding to the radius of the punch. The ratio of the punch radius (a_0) to the elastic layer thickness (h) provides a quantitative measure of sample confinement. Moreover, the stress distribution imposed by this geometry, shown in Fig. 2, has been quantified [5,17,18]. The nature of the debonding process can be related to the stress distribution at the surface of the cylindrical punch. Regardless of the confinement ratio, a singularity in the tensile stress exists at the edge of the cylinder. However, for low values of a_0/h, the stress decreases monotonically toward the center of the punch. As a_0/h increases, a second maximum in stress appears at the center of the punch, and the edge singularity becomes restricted to an increasingly

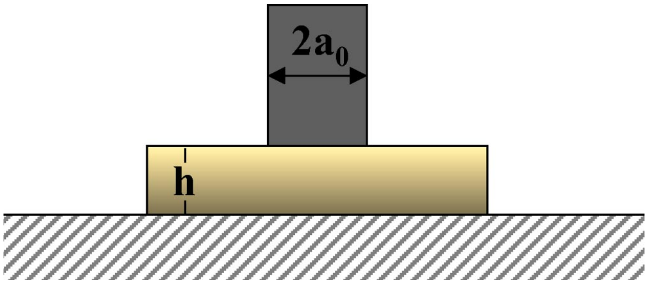

FIG. 1. The geometry of the adhesion test, a flat cylindrical punch with radius a_0 in contact with a thin elastic layer with thickness h. System confinement is defined as a_0/h.

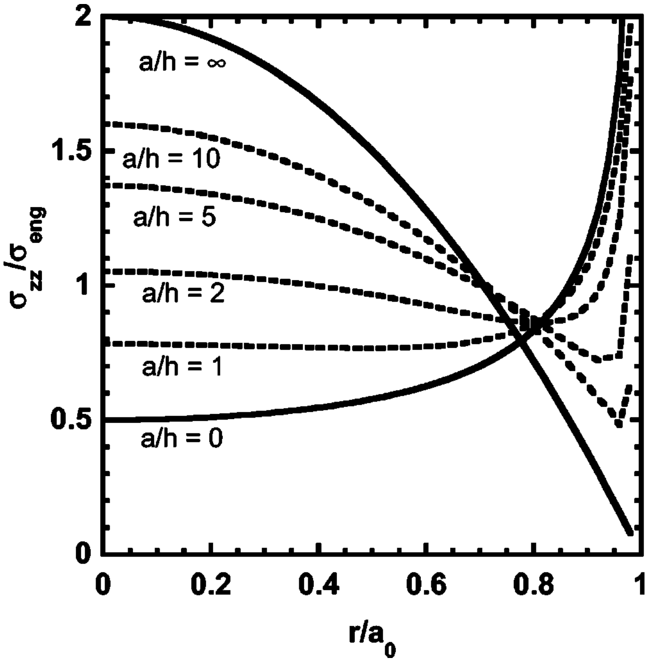

FIG. 2. The normal stress distribution for a flat punch in contact with a thin elastic layer as a function of confinement (a_0/h). The stress is normalized by the average tensile stress $(P/\pi a_0^2)$ [7].

smaller fraction of the punch surface.

This change in the nature of the stress distribution has a profound influence on the debonding mechanisms. For low values of a_0/h, the contact area remains circular, shrinking in size as the indenter is retracted from the elastic layer [5]. In this case, a circular crack propagating from the edge of the layer inward maximizes the compliance of the elastic layer for a given applied displacement and contact area. However, for thinner samples, the layer compliance is maximized for a more complicated deformation process. In many cases, the thin layer will cavitate internally to relieve the stresses under the center of the punch [17]. However, it is difficult for very soft materials, such as gels, to work against atmospheric pressure to achieve this. Fingerlike instabilities, which propagate along the interface (if adhesion is weak) or in the bulk (if adhesion is strong), occur instead. These different types of failure morphologies are apparent in soft gels at higher confinements where the confinement ratio a_0/h is greater than 1.

In this work, we investigate the behavior of confined systems using an axisymmetric probe tack test fitted with a flat-ended probe. The probe tack technique is a good method for investigating elastic instabilities in thin gels because both quantitative and qualitative information can be gleaned from the experiments. The data collected from this type of experiment allow a contact mechanics analysis to be used in interpreting results, giving detailed information about the mechanical and adhesive behaviors of the thin layers. The contact area images collected add a more qualitative understanding of the failure phenomenon by showing the progression of debonding throughout the test. Furthermore, the use of a cylindrical probe allows convenient access to a wide range of confinement ratios. In the following section, we outline the general compliance method used to analyze test results on thin gel layers, followed by a discussion of the debonding behavior for axisymmetric contact below a critical value of a_0/h. We then discuss the expected separation behavior above the critical value of confinement, making predictions for the mechanical behavior in this regime. We then describe our experimental results, categorized according to confinement values, in order to explore in detail the conditions for which contact is no longer axisymmetric.

II. COMPLIANCE METHOD

In analyzing probe tack experiments on thin gel layers, it is useful to consider the expression for stored elastic energy U for a system with a linear load-displacement relationship:

$$U=\frac{1}{2}\delta P=\frac{\delta^2}{2C}, \tag{1}$$

where P is the tensile load, δ is the tensile displacement, and C is the compliance of the thin layer. The general expression for the energy release rate $(\mathcal{G})$ follows from Eq. (1):

$$\mathcal{G}=\frac{\partial U}{\partial A}=-\frac{\delta^2}{2C}\frac{\partial C}{\partial A}=-\frac{P^2}{2}\frac{\partial C}{\partial A}, \tag{2}$$

where A is the circular area of contact between the layer and indenter. The energy release rate is the driving force for separation of the sample from the indenter. It can be viewed as the applied energy per area available to reduce the contact area by a unit amount, driving a crack forward and increasing the compliance of the layer [19]. The assumption in Eqs. (1) and (2) is that for a fixed contact geometry, the compliance is constant and defined as

$$C=\left.\frac{\delta}{P}\right|_A . \tag{3}$$

The gel used in these investigations has this characteristic [20], making Eq. (2) applicable for both circular and noncircular contact areas.

The critical energy release rate $(\mathcal{G}_c)$, a system parameter, represents the energy required to advance a crack during receding contact. For the gels in these experiments, $\mathcal{G}_c$ is nearly equivalent to the thermodynamic work of adhesion, the lower bound for $\mathcal{G}$ for a decreasing contact area [20,21]. For a given displacement, the contact area between the indenter and the elastic layer is determined by the requirement that $\mathcal{G}$ equals $\mathcal{G}_c$. The shape of this contact will be determined by the requirement that the compliance at a fixed contact area is maximized. If the contact remains circular and the elastic layer is incompressible, the compliance is approximated by

$$C=\frac{3}{8Ea}\left[1+1.33\frac{a}{h}+1.33\left(\frac{a}{h}\right)^3\right]^{-1}, \tag{4}$$

where E is Young's modulus of the layer and a is the radius of the actual contact area [21]. This equation was derived by fitting the finite element data of Ganghoffer and Gent [22]

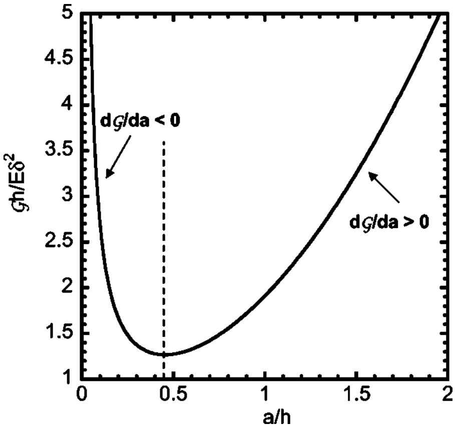

FIG. 3. Normalized energy release rate as a function of confinement. The minimum in the curve represents the critical value at which a/h begins to affect the separation behavior of a flat punch from an elastic layer.

and is valid for an incompressible elastic layer where $\nu=0.5$. As discussed in Sec. III, this assumption is valid for the gels utilized in our experiments. The energy release rate for axisymmetric crack propagation is obtained by combining Eqs. (1) and (3):

$$\mathcal{G}=\frac{2E\delta^2}{3\pi h}(a/h)^{-1}\left[1+2.67\left(\frac{a}{h}\right)+5.33\left(\frac{a}{h}\right)^3\right]. \tag{5}$$

Note that more general versions of Eqs. (4) and (5) valid for compressible elastic materials are also available [17,21,23], but are not necessary for our materials. Figure 3 shows a plot of Eq. (5) as a function of a/h. This curve experiences a minimum at $a/h=0.45$, where $\mathcal{G}=1.27E\delta^2/h$. The confinement ratio at the minimum in $\mathcal{G}$ represents a critical value separating qualitatively different detachment behaviors. Discussed below are the expected separation behaviors for different values of a_0/h; in all cases, the contact area is assumed to remain circular, with a single value of $\mathcal{G}_c$ characterizing the detachment. We also assume that the apparatus itself is much stiffer than the elastic layer, so that displacement applied to the elastic layer is directly controlled. This assumption is generally true for our gels, but the quantitative predictions need to be modified for highly confined layers with a sufficiently large elastic modulus. In these cases, the stored elastic energy in the device itself also needs to be taken into account [24,25].

A. $a_0/h=0$

The limiting case is a very thick, unconfined layer, for which a/h is effectively zero. Detachment occurs when $\mathcal{G}=\mathcal{G}_c$ at a displacement $\delta_{\max}$:

$$\frac{\delta_{\max}}{a_0}=\left(\frac{3\pi}{2}\right)^{1/2}\left(\frac{\mathcal{G}_c}{Ea_0}\right)^{1/2}. \tag{6}$$

Combining Eq. (3), Eq. (4) with $a/h=0$, and the definition of an average engineering stress $\sigma_{\mathrm{eng}}=P/\pi a_0^2$ leads to the relationship between engineering stress and normalized displacement for displacement values less than the maximum value:

$$\frac{\sigma_{\mathrm{eng}}}{E}=\frac{8}{3\pi}\frac{\delta}{a_0}. \tag{7}$$

A plot of σ_{eng}/E vs δ/a_0 forms a straight line with a slope of 0.85 that terminates at the value of $\delta_{\max}/a_0$ given by Eq. (6). During this stage, the energy release rate $\mathcal{G}$ is always lower than the critical value $\mathcal{G}_c$ and the contact radius does not change. At the point of maximum displacement, $\mathcal{G}$ becomes equal to $\mathcal{G}_c$ and the radius of contact decreases. Since, for this value of a_0/h, $\mathcal{G}$ increases with decreasing contact ratio, the system is unstable and, in the absence of viscoelastic dissipation, the radius of contact jumps from a_0 to zero.

B. $0<a_0/h<0.45$

For nonzero values of a_0/h that are below 0.45, the behavior is similar to the limiting case of $a_0/h=0$, despite the increased stiffness of the system. The contact radius jumps from a_0 to zero on separation. However, detachment occurs at a lower value of the maximum displacement. Also, the value of a_0/h now becomes important in determining the pull-off condition, obtained by setting $\mathcal{G}=\mathcal{G}_c$ in Eq. (5).

C. $a_0/h>0.45$

For a_0/h greater than the critical value of 0.45, the separation behavior becomes more complicated, as $\mathcal{G}$ decreases with decreasing contact radius. As a result there exists an equilibrium solution ($\mathcal{G}=\mathcal{G}_c$) to Eq. (5), and the contact area decreases at equilibrium during detachment. However, it is possible to predict the mechanical behavior by generating predicted tack curves, as long as the contact remains axisymmetric. Setting $\mathcal{G}=\mathcal{G}_c$, we can rearrange Eq. (5) to obtain

$$\frac{G_c}{Ea_0}=\frac{2\varepsilon^2}{3\pi\beta\alpha_0^2}\{1+2.67\beta\alpha_0+5.33\beta^3\alpha_0^3\}, \tag{8}$$

where $\varepsilon=\delta/h$ represents the effective strain, $\beta=a/a_0$ is a fractional contact radius describing the progression of the detachment, and α_0 is defined as the initial confinement (a_0/h). $\mathcal{G}_c/Ea_0$ is a meaningful dimensionless parameter that relates the importance of adhesive forces in a system to the contribution of the elastic strain energy for a semi-infinite elastic half space.

If values for $\mathcal{G}_c$, E, h, and a_0 are known, Eq. (8) can be solved to determine β at any value of the strain ε. Once β is known, the average engineering stress can be calculated from the following rearrangement of Eq. (3):

$$\frac{\sigma_{\mathrm{eng}}}{E}=\varepsilon\left\{0.85\frac{1}{\alpha_0}+1.13\beta^2+1.13\beta^6\alpha_0^2\right\}. \tag{9}$$

This situation is similar to the $a_0/h=0$ case where σ_{eng}/E is a linear function of displacement. Initially, σ_{eng}/E increases linearly with effective strain, $\mathcal{G}<\mathcal{G}_c$, and the slope is defined by the bracketed term in Eq. (9) with $\beta=1$ $(a=a_0)$. The

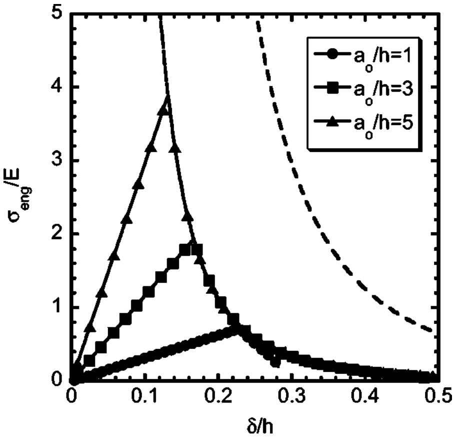

FIG. 4. Predicted tack curves for confinement values of 1, 3, and 5 ($\mathcal{G}_c/Ea_0=0.1$) plotted vs displacement normalized by thickness. The thickness remains constant, making the variation in confinement dependent on changing a_0. Two envelope curves for $\mathcal{G}_c/Ea_0$ values of 0.1 (dotted line) and 0.3 (dashed line) as a_0/h approaches infinity are also shown.

maximum in σ_{eng}/E occurs at the effective strain at which Eq. (8) is satisfied for $\beta=1$. After this point, β and σ_{eng}/E decrease until $a/h=0.45$, where pull-off occurs abruptly. Because pull-off occurs when $a=0.45h$, we can obtain an expression for this pull-off displacement δ^* by setting $\mathcal{G}=\mathcal{G}_c$ and $a=0.45h$ in Eq. (5):

$$\frac{\delta^*}{h}=0.89\left(\frac{\mathcal{G}_c}{Eh}\right)^{1/2}. \tag{10}$$

Three predicted tack curves, created by plotting values of σ_{eng} as a function of the effective strain ε, are shown in Fig. 4 for various confinement values. The confinement varies as a_0 is changed. Increasing a_0/h increases the maximum stress and changes the initial slope of the curves. However, after the maximum stress is reached, the curves all fall along the same equilibrium line for a given value of $\mathcal{G}_c/Ea_0$. Figure 4 displays two of these "envelope" curves for $\mathcal{G}_c/Ea_0$ values of 0.1 and 0.3. Since δ is normalized by h to give ε, a change in confinement corresponds to a fixed value of h and a change in a: the situation of a slow crack propagation at fixed $\mathcal{G}_c$. The predicted stress depends only on the current value of a, and not on its initial value a_0. An increase in the initial confinement (a_0/h) decreases the initial compliance of the layer and increases the stress required for the contact radius to begin shrinking.

Figure 5 displays predicted tack curves for the same values of confinement shown in Fig. 4. However, in this case, σ_{eng}/E is plotted as a function of δ/a_0. Plotting the curves in this way provides a simpler way of presenting the changes in the tack curves that are expected by varying h at a fixed value of a_0. For each of the three curves in Fig. 5 $\mathcal{G}_c/Ea_0=0.1$. As in the case of Fig. 4, the maximum stress increases with confinement. However, the shape of the curves now varies with a_0/h, indicating that the behavior depends on h. Although the shapes of the three curves in Fig. 5 are different, the areas under the curves are equal, determined by the constant value of $\mathcal{G}_c$ that is assumed. The area under each curve represents the energy required to separate the two surfaces and is equivalent to the energy release rate. To demonstrate this idea, we can equate the total mechanical energy put into the system with the energy required to separate the two surfaces [26]:

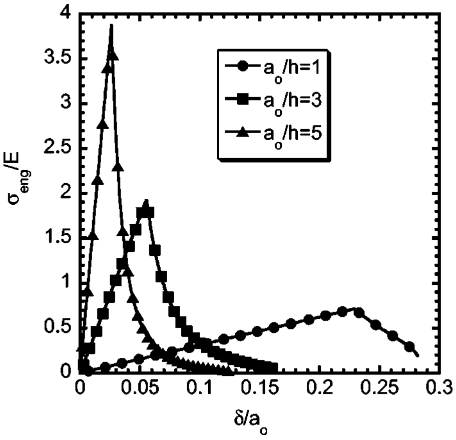

FIG. 5. Predicted tack curves for various confinement values plotted as a function of displacement normalized by initial contact radius. a_0/h changes as the thickness of the sample is varied, while a_0 remains constant.

$$\int P\,d\delta=\int \mathcal{G}\,dA. \tag{11}$$

If $\mathcal{G}$ is equal to $\mathcal{G}_c$ throughout separation, Eq. (10) can be rearranged to give

$$\mathcal{G}_c=\frac{1}{\pi a_0^2}\int P\,d\delta. \tag{12}$$

To relate this to the predictions in Fig. 5, we can rewrite this expression in the following form:

$$\frac{\mathcal{G}_c}{Ea_0}=\int \frac{\sigma_{\mathrm{eng}}}{E}d(\delta/a_0). \tag{13}$$

Figure 5 shows that, as confinement varies, the maximum displacement and stress change, while the area under the curve remains constant for a given $\mathcal{G}_c$. Detachment of indenter from the elastic layer occurs when $\delta=\delta^*$, with δ^* given by Eq. (10).

As discussed in more detail in the subsequent sections, the contact radius does not remain circular for $a_0/h>1$. Many of the results of this section remain valid, however, even when shape instabilities resulting in nonaxisymmetric contact are observed. These issues are discussed in more detail in Sec. IV.

III. MATERIALS AND METHODS

A schematic of the axisymmetric probe tack test apparatus is shown in Fig. 6. The test method, described in detail elsewhere, entails bringing a rigid indenter into and out of contact with the surface of a thin layer using a piezoelectric

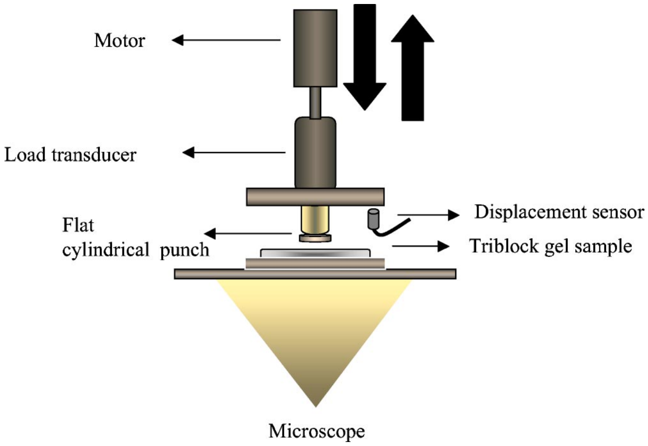

FIG. 6. A schematic of the probe tack apparatus for adhesion testing. The motor advances the punch into, and retracts it away from, the elastic layer while data are collected.

stepping motor [21,27]. Load and displacement data are collected through a load transducer and optical displacement sensor, while images of the area of contact between the indenter and the sample are captured by a video camera attached to an inverted microscope with a 2.5× objective lens. For the tests with $a_0/h<7$, the radius of the indenter (a_0) was generally 1.25 mm. The test with a confinement ratio of 25 was performed on a different apparatus, fitted with a device designed to adjust the parallelism between the film and the probe. This high confinement apparatus is similar in scope although slightly different in mechanical design [25].

The elastic layer used in these investigations is a physically cross-linked polymer gel, made by dissolving a triblock copolymer in 2-ethyl hexanol. The triblock has poly(methyl methacrylate) end blocks and a poly(*tert*-butyl acrylate) midblock with molecular weights of 29 000 and 100 000 respectively. The triblock copolymer was synthesized according to the methods of Varshney *et al.* [28] and has been described previously. The gel is a thermally reversible, low modulus elastic solid at room temperature with a gel point near 60 °C [20,21,29]. The volume fraction of copolymer in solution determines the modulus of the resulting gel. In this work, volume fractions between 0.036 and 0.2, corresponding to Young's moduli between 300 and 10 000 Pa, were used.

The gels have a finite osmotic compressibility, resulting in a time-dependent value of Poisson's ratio as solvent diffuses from regions of low to high hydrostatic tension. In order to develop a generalized framework for evaluating the importance of these effects in polymer gels, we utilize an analysis based on the value of the osmotic modulus K_{os} that is expected for these gels. The osmotic modulus is related to the concentration dependence of the osmotic pressure, which for semidilute solutions typically obeys a simple power law form [30]. The following specific expression accurately describes the concentration dependence of K_{os} for poly(α-methyl styrene) in toluene [31]:

$$K_{\mathrm{os}} \equiv \phi_p \frac{\partial \pi}{\partial \phi_p} \approx 6.60\times 10^6 \phi_p^{2.32} \quad (\mathrm{Pa}). \tag{14}$$

While the specific values of K_{os} vary to some extent from system to system, the values given by Eq. (14) are representative of most flexible polymers in good solvents. Values obtained for K_{os} for poly(methyl methacrylate) in a variety of solvents are very similar to the values given by Eq. (14), for example [32]. For the gels used in our experiments, we can estimate K_{os} from Eq. (14), where ϕ_p is the average volume fraction of the poly(t-butyl acrylate) midblock, for which 2-ethyl hexanol is assumed to be a good solvent.

For an isotropic material, Poisson's ratio is related to the ratio of the shear modulus to the bulk compressive modulus. An analogous osmotic Poisson ratio ν_{os} can be similarly defined in terms of G and K_{os} [33]:

$$\nu_{\mathrm{os}} = \frac{3-2(G/K_{\mathrm{os}})}{6+2(G/K_{\mathrm{os}})}. \tag{15}$$

Comparison of the measured values of G for our gels [20] to the predictions of Eq. (14), gives $G/K_{\mathrm{os}} \approx 0.1$, corresponding to a value of 0.45 for ν_{os}. This value corresponds to the ''relaxed'' Poisson ratio for the gel, over time scales long enough for the solvent distribution under the punch to equilibrate in response to the applied stress. The short-time value of the Poisson ratio is equal to 0.5, due to the incompressibility of the solvent itself. The transition between these time scales is determined by the collective diffusion coefficient of the gel, which for semidilute solutions can be written in the following form [34]:

$$D_c = \frac{k_B T}{6\pi \eta_0 \xi_h}, \tag{16}$$

where η_0 is the solvent viscosity (0.1 P for 2-ethyl hexanol at room temperature [35]) and ξ_h is the hydrodynamic screening length. For semidilute solutions of a polymer in a good solvent, the screening length can be expressed in the following scaling form [30]:

$$\xi_h = a \phi_p^{-0.75}. \tag{17}$$

Measured values of ξ_h for polystyrene in benzene [34] and polyacrylamide in water [36] are in good agreement with this prediction, with $a \approx 0.5$ nm.

From Eqs. (16) and (17), we expect $D_c \approx 10^{-7}$ cm^2/s for our gels. The longest experimental time scale in our experiments is about one minute, corresponding to a maximum diffusion distance $2(D_c t)^{1/2}$ of 40 μm, which is less than the thickness of even our thinnest layers, and much less than the lateral dimensions of the punch over which solvent must diffuse in order to modify the mechanical response of the layer. This same result can also be obtained by a mathematically equivalent analysis based on pressure driven flow of solvent through the gels [37–39].

While the analysis presented here neglects some quantitative details (we have neglected contributions of network elasticity to K_{os}, for example), the essential message is clear: the gels can be treated as incompressible solids with $\nu = 0.5$ on the time scale of our experiments. However, the presence of a substantial solvent fraction reduces viscoelastic

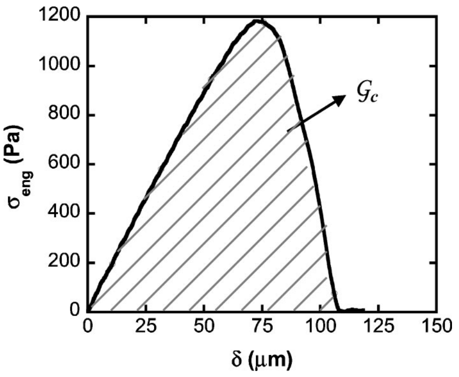

FIG. 7. The average stress-displacement curve for an elastic gel layer experiencing axisymmetric edge crack propagation $(a_0/h = 0.78)$. The indenter was advanced into the sample prior to the test; the data displayed were collected during retraction of the punch. The shaded area represents the critical energy release rate $(\mathcal{G}_c)$, in this case equal to the thermodynamic work of adhesion.

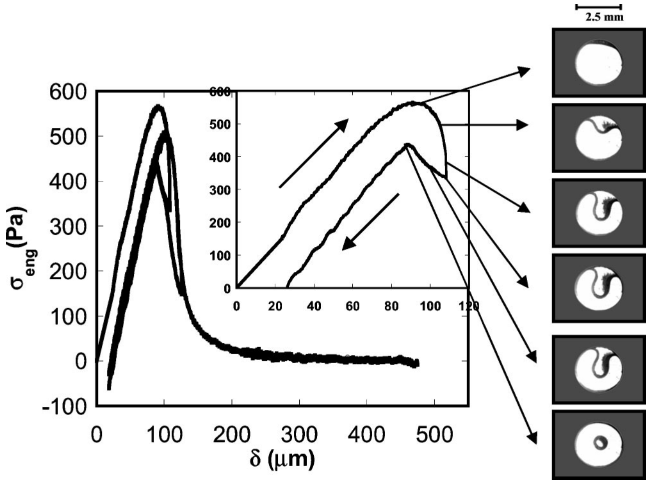

FIG. 8. The average stress-displacement curve for an elastic gel layer with $a_0/h = 1.93$. The inset shows the maximum stress peak reached during the first pull-off cycle. The images correspond to this peak, displaying the initiation and growth of a fingering instability, followed by the disappearance of the instability into a cavitated bubble as the indenter is pushed back into the layer.

effects so that the critical energy release rate is relatively insensitive to crack velocity and to polymer volume fraction. For the rates and concentrations of relevance here, $\mathcal{G}_c$ is equal to approximately twice the surface energy of 2-ethyl hexanol for a wide range of surfaces ($\mathcal{G}_c = 0.06$ J/m^2) [20]. This feature of the gels, together with their well-characterized structure and the ability to vary the modulus, shape, and size of the gel samples, makes them ideal model solids for these investigations.

IV. RESULTS AND DISCUSSION

In order to clearly demonstrate the effect of the confinement ratio, this section is divided into four subsections corresponding to different ranges of a_0/h.

A. $0.45 < a_0/h < 1$

For elastic layers with confinement ratios less than 1, the contact area remains circular during debonding, as expected for low values of a_0/h. Figure 7 shows a plot of stress versus displacement for a layer experiencing axisymmetric edge crack propagation, where contact remains circular ($a_0/h = 0.78$, $E = 10\,000$ Pa, and $h = 1.6$ mm). The test consisted of bringing the indenter into contact with the surface of the gel layer prior to testing and then retracting it out of contact. The shaded area under the curve represents the energy release rate for this test, 0.07 J/m^2. This value, calculated from Eq. (12), agrees well with the expected value.

B. $1 < a_0/h < 4$

Figure 8 displays a stress-displacement plot with the accompanying contact images for a gel layer with $a_0/h = 1.93$. The modulus and thickness of this layer are 1000 Pa and 647 μm, respectively. As expected from the stress distribution, preferred debonding was observed at the center of contact, although it occurred via an instability nucleating from the edge of the sample. The 2.5 cycles of receding and advancing contact that were imposed on this layer display the repeatability and consistency of the nonadhesive debonding process. The inset in the plot displays the maximum stress peak with arrows pointing to three receding contact images, during the nucleation of the instability, followed by three advancing contact images. During the first half cycle, debonding commences with the introduction of a finger from one edge, which slowly grows toward the center of contact. As the indenter is advanced back into the sample the first time, the finger shrinks and is pinched off, leaving a bubble-like region in the center that cannot be pushed out. The subsequent cycles progress in the same manner, with an instability growing in from one edge to join the central bubble during separation and then shrinking back on punch advance, leaving the bubble in place. The maximum stress during the first cycle represents the stress required to begin to decrease the contact area between the indenter and the gel. The maximum stress in subsequent cycles is lower because, once the central cavity is created, the stress required to continue debonding is less.

For these low modulus gels, the bubblelike cavity that remains after the instability is initiated can be thought of as a nearly incompressible inclusion with a shear modulus of zero. This can be demonstrated by considering the ratio p/E, the atmospheric pressure divided by the modulus of elasticity. For an ideal gas, the bulk compressive modulus describing the resistance to volume changes is equal to the pressure of the gas itself. In the case of the gel, p/E describes the hydrostatic stress required to change the volume of the gel relative to the deviatoric stress required to change the shape of the gel. If the value of this parameter is much larger than 1, atmospheric forces dominate over the stiffness of the gel, and the trapped bubble will change its shape but not its volume. For the triblock copolymer gels, p/E is between 20 and 100. It is because of the large value of this ratio that a central cavity is introduced via an edge instability rather than through cavitation of the gel in the center, which for low

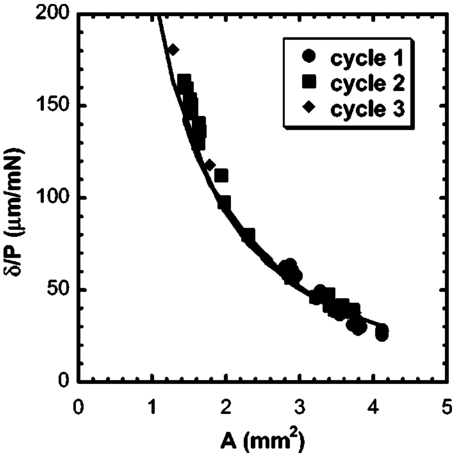

FIG. 9. Experimental compliance curves for an elastic gel layer with $a_0/h = 1.93$. A is the measured contact area. δ/P curves are shown for each of the 2.5 cycles. Cycle 3 represents the last half cycle of the experiment. The solid line depicts the axisymmetric compliance determined from Eq. (4) and assuming a circular contact with the same total area as the irregular contact ($A = \pi a^2$).

values of p/E occurs for $\sigma_{\mathrm{eng}}/E > \sim 1$ [7,18]. The gel cannot overcome compressive atmospheric forces to form internal voids. This accounts for the compliance and displacement offset effects observed in the experimental data. The central bubble, acting as an inclusion, restricts compression of the gel back to zero displacement, resulting in a displacement shift.

It is useful at this point to distinguish between open and closed detachment zones. In Fig. 8, the top five images display open detachment zones in which debonding propagates from the edge and the detachment zone is accessible to the atmosphere. The bottom image in Fig. 8 displays a closed detachment zone, in which detachment has occurred between the sample and indenter, but the detachment zone is not open to the atmosphere. It is the closed detachment zones that behave as the incompressible inclusions described above. They form because, for a given value of the contact area, this particular geometry minimizes the total elastic energy of the system.

Figure 9 displays experimental compliance curves for each cycle of this sample ($a_0/h = 1.93$). Experimental compliance is represented by δ/P from Eq. (3), and the contact areas plotted on the x axis are established through analysis of the contact area images. In calculating the experimental compliance for cycles 2 and 3, an offset of 25 μm is included in the displacement values to account for the presence of the closed detachment zone that is introduced (see inset of Fig. 8). The same relationship between compliance and contact is observed for each cycle. Additionally, the δ/P values are only slightly larger than the compliance values for a circular contact zone with the same total area, given by Eq. (4) and shown by the solid curve in Fig. 9. This very small increase in compliance is responsible for the dramatic change observed in the contact behavior. In other words, this shows that the compliance of the layer in this weakly confined regime is only weakly affected by the detailed shape of the contact area. Interestingly, an identical conclusion has been obtained for the case where the elastic layer is replaced by a Newtonian fluid [14].

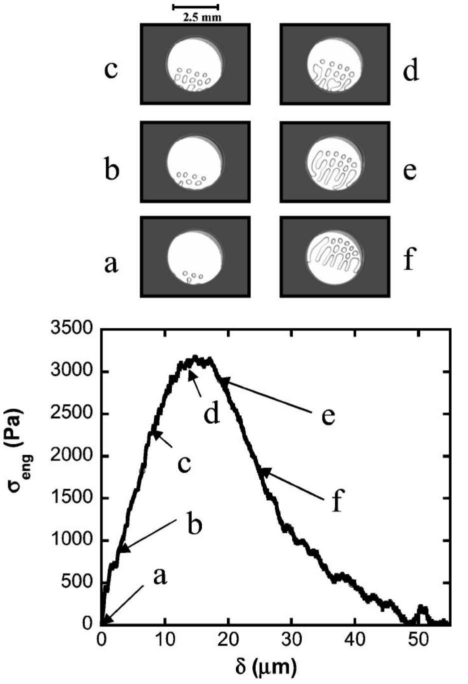

FIG. 10. The average stress-displacement curve for a layer with $a_0/h = 6.07$. The images correspond to the curve, displaying the onset and growth of fingering instabilities.

C. $a_0/h > 4$

The stress-displacement curve for a more highly confined sample ($a_0/h = 6.07$) is shown in Fig. 10. In this case, the indenter was pulled out of initial contact with the layer until separation. The Young's modulus of this layer is 5000 Pa, while its thickness is 206 μm. The images accompanying the stress-displacement curve show contact instabilities beginning to nucleate from one side of the punch before the stress maximum is reached. The asymmetry of the detachment is attributed to the difficulty in perfectly aligning a flat indenter with respect to the sample surface. Both open and closed detachment zones are apparent in the images in Fig. 10. Multiple instabilities move in from the edge of the sample as the punch is retracted. From Fig. 10, it is evident that thinner samples have more and smaller fingerlike instabilities. As discussed in more detail below, our observation that the size of these instabilities is directly related to the thickness of the layer is consistent with other experiments using highly confined systems with nonaxisymmetric geometries [3,4,6].

Figure 11 displays δ/P values plotted against the measured contact areas for this sample ($a_0/h = 6.07$). As in Fig. 9, the experimental compliance for the noncircular contact geometry (δ/P) is compared to the compliance prediction given by Eq. (4), which assumes a circular contact. The experimental compliance (symbols) is clearly higher than the compliance for a circular contact area of the same size (solid line). The fingering instabilities maximize the compliance of the gel layer beyond what axisymmetric debonding could achieve, reducing the stored elastic energy.

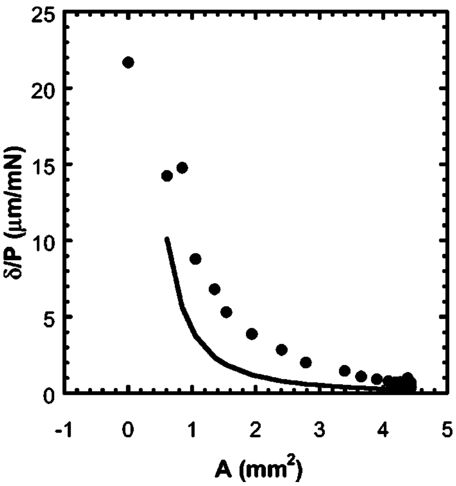

FIG. 11. Curves of experimental and predicted compliance for a layer with $a_0/h=6.07$. A is the measured contact area. The δ/P curve (dots) is higher than the predicted axisymmetric compliance from Eq. (4) (solid line), displaying that the instabilities introduced during debonding maximize the compliance of the thin layer.

Not only is the compliance treatment useful in quantifying the difference in behavior observed in confined systems, but with the same equations it is possible to generate contact area values directly from measured load and displacement data. Using experimental load and compliance values from Eq. (3), Eq. (2) can be used to determine either $\mathcal{G}_c$ or A. For the case in which $\mathcal{G}_c$ is known, a contact area profile can be determined by plotting $P^2/2\mathcal{G}_c$ as a function of compliance and integrating this curve to calculate the change in A at each point along the load-displacement curve:

$$A(\delta=\Delta)=\pi a_0^2-\frac{1}{2\mathcal{G}_c}\int_{\delta=0}^{\Delta}P^2(\delta)d(\delta/P). \tag{18}$$

Using this approach, it is possible to determine the amount of material in contact with the indenter at any point during debonding without actually seeing the contact area. Note that the contact area does not need to remain circular in order for this approach to be valid, since no assumptions are made about the detailed nature of the compliance function. The only assumption is that for a given contact geometry the relationship between load and displacement is linear.

Figure 12 compares the measured and calculated contact areas for the sample with $a_0/h=6.07$. The contact areas calculated using Eq. (18) are in good agreement with the actual areas measured from the contact images. This straightforward analysis is possible when the energy release rate is known and does not vary with crack velocity over the range of values tested. This criterion is met for the gels discussed here, but it is not satisfied for elastomeric materials in general [40]. For this reason a quantitative analysis of the behavior of confined viscoelastic solids is much more complicated.

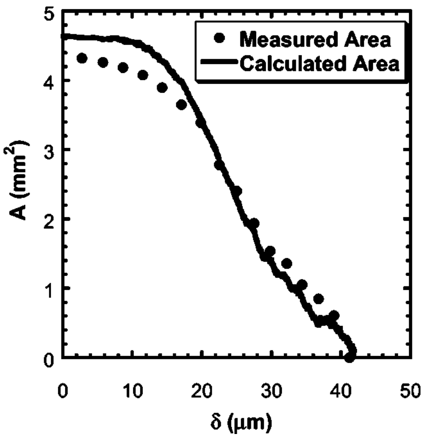

FIG. 12. Measured and calculated areas plotted against experimental displacement. The calculated area curve is determined from Eq. (18), using the experimental load and compliance and assuming $\mathcal{G}_c=0.06$ J/m^2.

D. $a_0/h>20$

Figures 13 and 14 display a stress-displacement curve and the accompanying contact area images for a very soft highly confined layer ($a_0/h=25$, $E\sim 300$ Pa, $h=100\ \mu$m, $a_0=2.5$ mm) in which instabilities are also observed on advancing contact. During this test, the cylindrical indenter was advanced into the layer and then retracted until complete separation. In Fig. 14, the first four images display the progression of advancing contact, while the bottom-most image was taking during punch retraction. As the punch advances into the sample, initial contact is made at an asperity, after which the contact grows by the appearance of fingers with wavelengths on the order of a few times the layer thickness. The fingers eventually form channels that pinch off to form voids, which are pushed to the edge of contact as the punch continues to compress the layer. During pull-off, the void motion reverses toward the center of contact, followed by the propagation of fingers from the edge that grow together to achieve complete separation. Again, both open and closed detachment zones appear during the course of the experiment, and the experiment is reversible.

The methodology described in Sec. II C to predict tack curves cannot be extended to the very large values of a_0/h that result in contact geometries similar to that illustrated in Fig. 14. This type of contact cannot be viewed simply as a

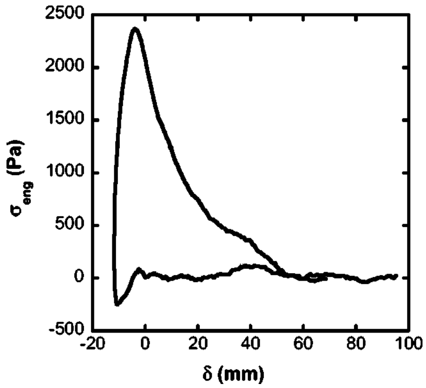

FIG. 13. The average stress-displacement curve for a gel layer with $a_0/h=25$. The indenter was advanced into the layer and then retracted until complete separation.

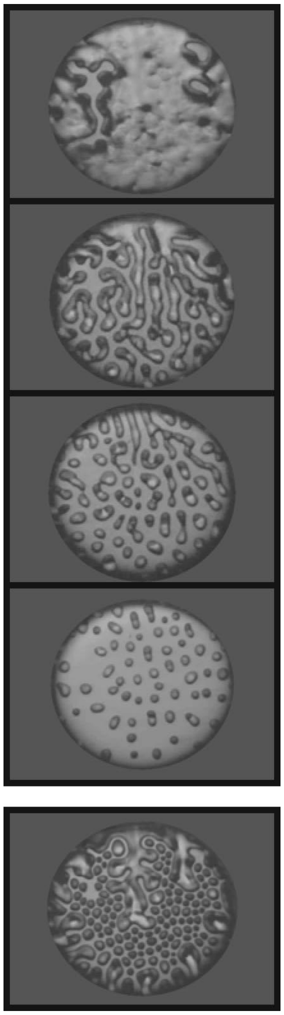

FIG. 14. Contact images corresponding to the curve shown in Fig. 13. The first four images were taken during advancing contact, while the last image shows the morphology observed during receding contact.

circular contact that is modified by detachment fingers that propagate from the edges. For the expected limiting behavior for $a_0/h \rightarrow \infty$, a critical displacement exists, above which one expects complete detachment to occur. This critical displacement δ^* can be estimated by a procedure outlined by Mönch and Herminghaus [6], which is closely related to the previous treatment of Ghatak *et al.* [3]. These authors considered the elastic energy required to impose the following sinusoidal displacement on an elastic film of thickness h:

$$\delta = \delta_0 \sin(2\pi x/\lambda). \tag{19}$$

For an incompressible film (Poisson's ratio $= 0.5$), the elastic strain energy associated with this perturbation is

$$U(q) = \frac{A_0 \delta_0^2 E q}{6h} \frac{\cosh^2(q) + q^2}{\sinh(q)\cosh(q) - q}, \tag{20}$$

where $q = 2\pi h/\lambda$ and A_0 is the total interaction area between the two surfaces (πa_0^2 for a flat punch of radius a_0). In our case fingering appears during contact with the indenter. By approximating the contact as a sine wave, we take $\delta = \delta_0$ and obtain the following expression for the compliance of the film by comparing Eq. (20) to Eq. (1):

$$C(q) = \frac{3h}{\pi a_0^2 E q} \frac{\sinh(q)\cosh(q) - q}{\cosh^2(q) + q^2}. \tag{21}$$

The compliance is maximized at $q = 2.12$, $(\lambda/h = 2.96)$, where it has the value of $0.964h/A_0 E \approx h/A_0 E$.

An expression for the pull-off displacement can be obtained by approximating the actual contact area as half the apparent contact area of the punch ($A = A_0/2$),

$$C = \frac{h}{2AE}. \tag{22}$$

This form of the compliance can be combined with Eqs. (2) and (3) (with $\mathcal{G} = \mathcal{G}_c$) to give an expression for the pull-off displacement δ^*:

$$\delta^*/h = (\mathcal{G}_c/Eh)^{1/2}. \tag{23}$$

Apart from a small difference in the prefactor, this value is identical to the pull-off displacement given by Eq. (13), obtained by assuming pull-off occurs when a circular contact zone shrinks to give a radius of $0.45h$. This result can be explained by the fact that the fingering instability separates the contact into zones that behave in some ways as if they are mechanically independent. Adhesive detachment for a highly confined system therefore occurs in the following manner. The load initially increases very quickly as the imposed displacement is increased. For an incompressible system, the compliance is given by Eq. (4). For high values of p/E, the compliance is eventually increased by the appearance of detachment fingers that propagate in from the edges of the punch. For low values of p/E, the compliance is increased by internal cavitation. In either case, Eq. (22) provides an upper value for the compliance, representative of a contact geometry in which the fingering, or internal debonding resulting from cavitation, is fully developed. In general, the compliance will be intermediate between these two extremes, and increases throughout the test from the value given by Eq. (4) to the value given by Eq. (22). Detachment occurs at $\delta = \delta^*$ in both cases. The initial slope, final pull-off displacement, and integrated areas of the tack curves shown in Figs. 4 and 5 are representative of the actual tack curves, but the fingering instabilities cause the real tack curves to be more rounded, with a lower value of the maximum stress than the value that is predicted.

E. Characteristic dimensionless parameters

The overall deformation behavior of thin compliant systems is determined by several dimensionless quantities. The first of these is a_0/h, which describes the geometric confinement of the system, and $\mathcal{G}_c/Ea_0$, which describes the importance of adhesive forces relative to elastic forces. These parameters have been combined to give a failure map describing the deformation modes experienced by elastic layers [7]. For samples in which internal cracks are not present, the deformation modes are edge crack propagation, corresponding to adhesive failure propagating from the edge of the contact zone, and bulk instabilities, typically corresponding to internal cavitation. A transition from edge crack propagation to cavitation occurs when the average stress applied to adhesive material exceeds the elastic modulus. An implicit assumption in this prior treatment is that p/E, the ratio of the external pressure to the elastic modulus of the material, is not substantially greater than unity. Higher values of p/E suppress internal cavitation, so that edge crack propagation proceeds at values of the average stress that can be well in excess of the elastic modulus of the layer. Also, only ‘‘circular’’ edge crack propagation was considered in Ref. [7], as opposed to the fingering modes that are described above. The detailed deformation behavior of very soft elastic layers is actually quite rich and must be represented by a deformation map of at least three dimensions, with p/E, a_0/h, and $\mathcal{G}_c/Ea_0$ representing the three orthogonal axes.

Finally, it has been assumed to this point that the deformation behavior is entirely determined by the balance between the elastic energy associated with deformation of the layer and the adhesion energy required to separate it from a surface. Analysis of this problem for very large values of a_0/h predict characteristic wavelengths of the adhesive instabilities that are 3.96 times the elastic layer thickness [6]. While this value is qualitatively consistent with the results that we have obtained, some quantitative differences can be attributed to the energy required to deform the free surface. This energy is related to a ratio involving the elastic modulus of the layer and the Laplace pressure associated with curvature of the free surface. For very large values of a/h, this curvature is controlled by h, so that the characteristic Laplace pressure is comparable to γ/h. The quantity γ/Eh therefore emerges as an additional dimensionless parameter that describes the importance of surface energy relative to the deformation energy. We have made the implicit assumption in our analysis that γ/Eh is small. In fact, because $\mathcal{G}_c \approx 2\gamma$ for our gels, $\gamma/Eh \approx 2(\mathcal{G}_c/Ea_0)(a_0/h)$, a quantity that varies between 0.06 and 2 in our case. While we do not believe that these values of γ/Eh are large enough to substantially modify the results that we have obtained, they will affect the details, resulting in an increased value of the characteristic wavelength of the adhesive instabilities [6].

V. CONCLUSIONS

The effect of confinement on the debonding behavior of compliant elastic layers has been investigated. The behavior that manifests during interfacial debonding is dependent on the layer thickness, with more highly confined samples experiencing fingerlike interfacial instabilities. The origins of these instabilities can be related to the nature of the stress distribution within the layer. A compliance-based fracture mechanics analysis has been applied to experimental data in order to quantify the underlying physics of the debonding morphologies. The various confinement-dependent behaviors for different a_0/h ranges have been elaborated, and the experimental debonding behaviors for increasing values of a_0/h have been described.

In order to express our results in an appropriately generalized form, we have defined the following four dimensionless parameters that play an important role in determining the separation behavior of thin elastic layers.

(1) a_0/h. The ratio between the punch radius and the adhesive layer thickness determines the stress distribution under the punch. Fingering instabilities in the shape of the crack front are observed for $a_0/h > 1$.

(2) $\mathcal{G}_c/Ea_0$. This ratio describes the relative importance of adhesive forces. For highly confined systems, the adhesive layer thickness is a more natural length than the punch radius a_0, and a more natural dimensionless group is $\mathcal{G}_c/Eh$. The square root of this quantity gives the overall effective strain that can be applied to the adhesive layer prior to detachment.

(3) p/E. The ratio of the atmospheric pressure to the elastic modulus determines the system’s potential for internal cavitation. If the value of this parameter is much larger than 1, internal cavitation is suppressed. Internally debonded areas appear at high values of a_0/h by the propagation of fingers from the edge of the contact zone. If these fingers pinch off so that the cavities are no longer open to the external environment, they behave as incompressible inclusions, provided that $p/E \gg 1$.

(4) γ/Eh. This quantity relates the energy required to deform the free surface of the material to the elastic energy required to deform the bulk of the material. While the characteristic wavelength of the adhesive fingering instability is expected to increase for large values of this quantity, the qualitative features of the debonding process are not strongly affected for $\gamma/Eh < 1$.

ACKNOWLEDGMENT

This work was supported by the National Science Foundation under Grant No. 0214146.

[1] C. Creton, in *Processing of Polymers*, Vol. 18 of *Materials Science and Technology* edited by H. E. H. Meijer (VCH, Weinheim, Germany, 1997), p. 707.

[2] N. A. Peppas and J. J. Sahlin, Biomaterials **17**, 1553 (1996).

[3] A. Ghatak *et al.*, Phys. Rev. Lett. **85**, 4329 (2000).

[4] V. Shenoy and A. Sharma, Phys. Rev. Lett. **86**, 119 (2001).

[5] K. R. Shull, C. M. Flanigan, and A. J. Crosby, Phys. Rev. Lett. **84**, 3057 (2000).

[6] W. Mönch and S. Herminghaus, Europhys. Lett. **53**, 525 (2001).

[7] A. J. Crosby *et al.*, J. Appl. Phys. **88**, 2956 (2000).

[8] A. Sharma and R. Khanna, Phys. Rev. Lett. **81**, 3463 (1998).

[9] G. Reiter, R. Khanna, and A. Sharma, Phys. Rev. Lett. **85**, 1432 (2000).

[10] S. Poivet *et al.*, e-print cond-mat/0210064.

[11] E. Lemaire *et al.*, Phys. Rev. Lett. **67**, 2009 (1991).

[12] P. Coussot, J. Fluid Mech. **380**, 363 (1999).
[13] A. Lindner, P. Coussot, and D. Bonn, Phys. Rev. Lett. **85**, 314 (2000).
[14] D. Derks *et al.*, J. Appl. Phys. **93**, 1557 (2003).
[15] P. G. Saffman and G. Taylor, Proc. R. Soc. London, Ser. A **245**, 312 (1958).
[16] C. Creton, J. Hooker, and K. R. Shull, Langmuir **17**, 4948 (2001).
[17] C. Creton and H. Lakrout, J. Polym. Sci., Part B: Polym. Phys. **38**, 965 (2000).
[18] C. Fond, J. Polym. Sci., Part B: Polym. Phys. **39**, 2081 (2001).
[19] J. G. Williams, *Fracture Mechanics of Polymers* (Halsted Press, New York, 1984).
[20] C. L. Mowery *et al.*, Langmuir **13**, 6101 (1997).
[21] K. R. Shull *et al.*, Macromol. Chem. Phys. **199**, 489 (1998).
[22] J. F. Ganghoffer and A. N. Gent, J. Adhes. **48**, 75 (1995).
[23] Y. Y. Lin, C. Y. Hui, and H. D. Conway, J. Polym. Sci., Part B: Polym. Phys. **38**, 2769 (2000).
[24] M. Barquins and D. Maugis, J. Adhes. **13**, 53 (1981).
[25] G. Josse *et al.* (unpublished).
[26] K. R. Shull, Mater. Sci. Eng., R. **36**, 1 (2002).
[27] D. Ahn and K. R. Shull, Macromolecules **29**, 4381 (1996).
[28] S. K. Varshney *et al.*, Macromolecules **24**, 4997 (1991).
[29] C. M. Flanigan, A. J. Crosby, and K. R. Shull, Macromolecules **32**, 7251 (1999).
[30] P.-G. de Gennes, *Scaling Concepts in Polymer Physics* (Cornell University Press, Ithaca, NY, 1979).
[31] I. Noda *et al.*, Macromolecules **14**, 668 (1981).
[32] H. Vink, Eur. Polym. J. **10**, 149 (1974).
[33] I. M. Ward and D. W. Hadley, *An Introduction to the Mechanical Properties of Solid Polymers* (Wiley, New York, 1993).
[34] M. Adam and M. Delsanti, Macromolecules **10**, 1229 (1977).
[35] C. Marsden and S. Mann, *Solvents Guide* (Interscience, New York, 1963).
[36] E. Geissler and A. M. Hecht, Macromolecules **14**, 185 (1981).
[37] A. M. Hecht and E. Geissler, Polymer **21**, 1358 (1980).
[38] E. Geissler and A. M. Hecht, J. Chem. Phys. **77**, 1548 (1982).
[39] G. W. Scherer, J. Non-Cryst. Solids **142**, 18 (1992).
[40] D. Maugis and M. Barquins, J. Phys. D **11**, 1989 (1978).